Passive Vibration-Sensing System Using Hybrid Alignment Nematic Liquid-Crystal Gratings

Xinyi Yu, Oleksandr Semenenko, Valerii Vashchenko, Abhishek Kumar Srivastava

State Key Laboratory of Advanced Display and Optoelectronics, and Centre for Display Research, Department of Electronic and Computer Engineering, Hong Kong University of Science and Technology Hong Kong University of Science and Technology, Hong Kong

Abstract

Unlike the commonly used electrically controlled birefringence mode liquid crystals, hybrid alignment nematic (HAN) liquid crystals eliminate the threshold voltage. Therefore, they have excellent application prospects in low-voltage photonic components. This article discloses a power-free vibration detection system based on optical fiber, HAN, and a passive vibration transducer. Using the photoalignment techniques, we fabricated HAN grating cells and deployed them into the vibration sensing system, achieving a sensitivity of 13.1 rad/m/s. Meanwhile, we measured the frequency response and resolution and analyzed its performance in actual conditions. The system has excellent cost-efficiency and optimization spaces, which can be applied in large-scale vibration monitoring in the field.

Author Keywords

Liquid crystal; vibration sensing; hybrid alignment; liquid crystal grating; passive sensing.

1. Introduction

Sensors play a pivotal role in the development of digital twins and smart cities [1], with increasing demand and new requirements from the market for cost and lifetime. Among them, vibration sensors are widely used in work status monitoring [2] and intelligent traffic management [3], especially for monitoring potential safety hazards in buildings [4] and natural disasters [5], providing real-time early warnings. Moreover, large-scale vibration sensing arrays can reduce costs and workload in fields such as structural health monitoring (SHM), offering real-time and precise diagnostics [4]. However, its deployment and maintenance are costly, especially in harsh environments where power supply and lifespan are a big concern. Energy-harvesting technologies such as photovoltaics, wind energy, and triboelectric generation [6] have partially addressed the anxiety overpowering endurance, but these power elements often require maintenance.

Passive vibration sensing using magnetoelectricity and piezo-electricity can convert vibration energy into electrical signals without an external power source. They are structurally straightforward and more cost-effective, eliminating power endurance, but the produced electrical signals are very weak. Once transmitted over long distances, the transmitted signal can lose vital information due to the poor signal-to-noise ratio (SNR) of the unamplified raw signals. Therefore, in oceanic seismic, land geological, remote artificial structure monitoring, passive sensors are not applicable.

Fiber Bragg grating (FBG) is another approach to make highly sensitive passive vibration sensing, already applied in sonar and seabed mining [7]. Although seabed seismic networks like the NEPTUNE project can monitor earthquakes over the long term [8], they are too costly. In 2018, British researchers used commercial fiber optics and laser interferometry to detect earthquakes at a lower cost [9], but this method can hardly locate the vibration source, limiting its application in SHM and early warning.

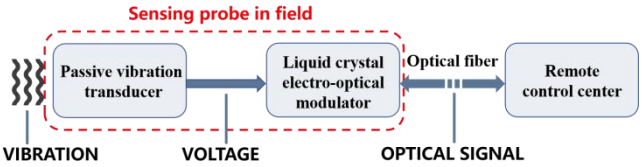

Figure 1. The concept diagram of the proposed passive sensing system.

Therefore, the current challenges prompt us to propose a combined solution of passive vibration transducers (PVT) - threshold-less liquid crystal electro-optic (EO) modulators - optical fibers. As shown in Fig. 1, PVT converts vibrations into weak voltage signals to drive the liquid crystal (LC) in modulators, modulating the phase or intensity of impinging optical signals from optical fibers. The signal is transmitted back to the control center via optical fiber for processing and analysis. In 2022, we fabricated a preliminary sensing system using deformed helix ferroelectric liquid crystal (DHFLC) and piezoelectric films and calibrated the system sensitivity using a reciprocating motion machine. The results confirmed the feasibility of our solution. However, further research confirmed that due to the small size of the mass block and the high stiffness of the piezoelectric film, the frequency response only covers >100 Hz and is uneven, which is unfavorable for SHM and seismic detection focused on the 0.1-100 Hz range. Therefore, we shift to hybrid alignment nematic (HAN) liquid crystals and mature magnetoelectric PVT in this article. We calibrated and analyzed the system output and verified its feasibility in SHM.

2. Experiments

The pre-tilt angle is defined as the angle between the LC easy-axis and the substrate. Electrically controlled birefringence (ECB) nematic liquid crystal (NLC) cells with an anti-parallel planar alignment (PA) and a pre-tilt angle of 0-10 ° typically possess a threshold voltage (V_{th}) of 1-2 V due to the Fredericks transitions. Therefore, when the applied voltage is less than V_{th}, the NLC cells have no optical response. The definition of V_{th} is [10]:

$$V_{th} = \pi\sqrt{K_{ii} / \varepsilon_0 \Delta\varepsilon}$$

where K_{ii} is the elastic constant, $\Delta\varepsilon$ is the dielectric anisotropy of LC, and ε_0 is the vacuum permittivity. V_{th} can be reduced by increasing $\Delta\varepsilon$, but the viscosity of the NLC also increases, thereby slowing down the response. Therefore, we adjust V_{th} by controlling K_{ii}, such as changing the alignment type of the LC cell.

The hybrid alignment nematic (HAN) LC cell was first proposed in 1976, where the top and bottom substrates are vertical (VA) and planar alignment, respectively. [11] Ideally, the director of the molecules tilt uniformly from 0° to 90° in the LC layer (Fig. 2(a)). This unique arrangement of LC molecules eliminates the

ISSN 0097-996X/25/5603-2166-$1.00 © 2025

V_{th}, which is very suitable for the proposed application. However, the phase retardation of HAN cells is only about half that of PA cells with the same gap. [11]

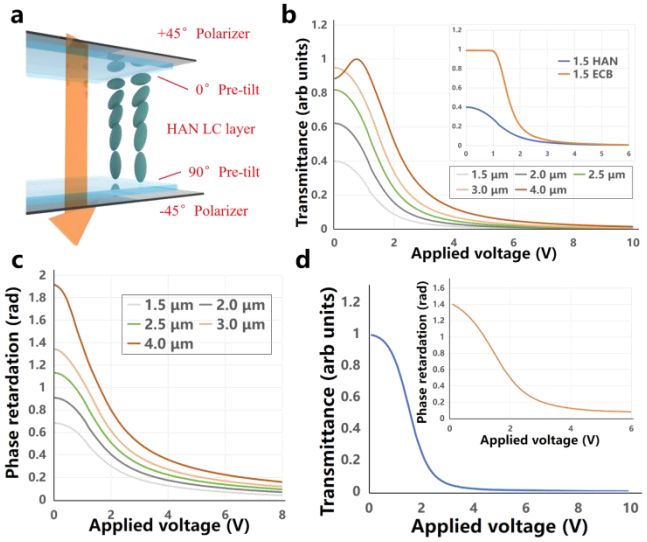

Figure 2. (a) A schematic diagram of the LC molecules distribution in a HAN cell. (b) A comparison of ECB and HAN cell of the same cell gap and TVCs of HAN cells with different cell gaps. (c) The phase retardation of HAN cells with different cell gaps. (d) The TVC and phase of a fabricated HAN cell.

Therefore, we compared the transmission versus voltage (TVC) curve and phase retardation of different cell gaps and cell types in transmission mode at 632 nm wavelength using Mouse-LCD simulation software, helping us select the best cell gap. In the simulation, we set the pre-tilt angles on both sides of the HAN cell as 0° and 90°, respectively. Both sides of the PA ECB cell are 0°; The LC layer material is E7 (Δn = 0.2082 @ 632nm). Insert in Fig. 2(b) compares the different optical responses of two cells with the same gap of 1.5 μm. Compared with ECB, HAN eliminates the influence of V_{th}. Both Fig. 2(b) and (c) indicate that before a HAN cell reaches the $\pi/2$ delay, as its gap increases, the range of modulated light intensity and phase delay increase, which is beneficial for improving the system sensitivity and resolution. In addition, 2(c) indicates that larger gaps provide longer and better linear response regions. However, when the delay is greater than $\pi/2$, such as '4.0 μm' in (b), the cell exhibits a non-monotonic intensity response. Therefore, theoretically, for EO modulators, a cell with exactly $\pi/2$ delay can provide the largest modulation depth and linear phase response. If we use E7 for a 632 nm optical system, the cell gap is ~3.2 μm. We used ball spacers of 3 μm diameter in subsequent experiments.

As shown in Fig. 3(a), we deposited a VA material chromolane used in the previous work [12] onto a ITO coated glass substrate. Then, we used the method shown in the work [13,14] to coat cinnamate phosphonic acid (CPA) on the other substrate as a photosensitive PA layer. After linear polarized UV light irradiation, CPA can provide a nearly 0° pre-tilt angle without multi-domain alignment. CPA is also suitable for HAN grating (HANG), which can provide various sizes of patterned alignment through multiple-exposure with shadow masks. Two exposures have different polarization directions, with preferred directions of 0° and 45°. In Fig. 3(e), we took 10-μm-pitch checkerboard grating that diffracts the light and detected the 0-order diffraction light, which increases at relatively larger applied voltages. The effective area of the cell was reduced to 4 × 4 mm^2 to minimize the cell's capacitance and improve its response speed. We separated two substrates with spacers to assemble a cell, and injected E7 and connected wires. We used the setup in Fig. 3(c) to test the HAN cell's EO response, where the cell was placed at 45° between the crossed polarizers. The TVC and phase retardation of the cell are shown in Fig. 2(d), which is consistent with the simulation results. Similarly, the setup in Fig. 3(g) was for HANG, from which we got a threshold-less linear TVC as Fig. 3(f).

Meanwhile, two setups were also used as the EO modulator in the proposed system. A 632 nm semiconductor laser simulates the light from the optical fiber, and the signal receiver 'control center' is replaced by a free-space biased detector (DET36A2, Thorlabs). The entire set was packaged in a ground-connected metal box to achieve light and electromagnetic shielding. The electrical signal from PVT is applied to the cell, while the modulated light intensity signal is output from the detector. We used a magnetoelectric PVT from Shanghai Nuxing Automation

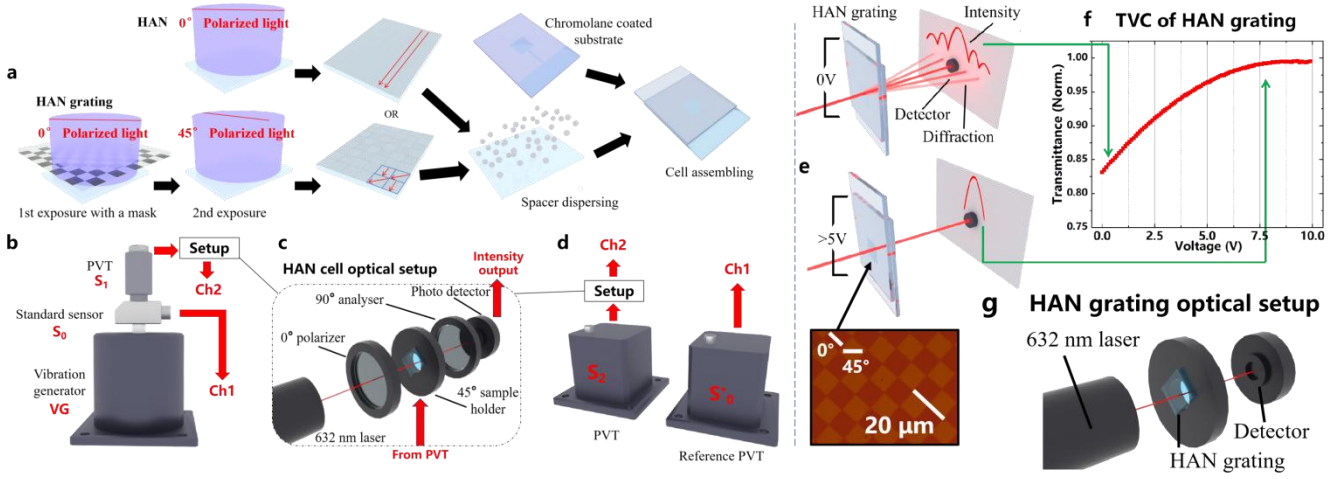

Figure 3. (a) The fabrication details of HAN and HANG cells. (b) An abridged view of system standardization setup, where the standard sensor (S_0) is oscilloscope channel 1 (Ch1) and PVT (S_1) drives the HAN optic setup and output to Ch2. (c) The optic setup containing a HAN cell. (d) A view of the setup for natural vibration testing, where the reference PVT (S'_0) is Ch1 and PVT (S_2) drives the HAN optic setup and output to Ch2. (e) The mechanism of HANG. (f) The TVC of a HANG cell. (g) The optic setup contains an HANG cell.

Equipment Co., Ltd, NX-0801 (10-1000 Hz, 50 mV/mm/s, ±5%), and a 941B (0.25-80 Hz, 0.3 V/m/s^2, ± 1/3dB) from Zhejiang Boyuan Electronic Technology Co., Ltd, to measure the system's frequency response and actual performance, respectively. The PVT connected EO modulator represents the sensing probe installed in the field, referring to the red rectangle area in Fig. 1.

3. Results and discussions

For HAN cells, as is shown in Fig. 3(b), when measuring the system's sensitivity, range, and frequency response (FR), the NX-0801 ($\mathbf{S_1}$) was rigidly installed with a standard sensor, Integrated Electronics Piezo-Electric (IEPE) mode velocity sensor 311V01-25.4 (0.2 V/mm/s, 5 - 1000 Hz, ± 5%) ($\mathbf{S_0}$) on the vibration generator SA-JZ002 (Wuxi Shiao Technology Co., Ltd) (**VG**), which can produce sinusoidal periodic vibrations raging from 1.6 Hz to 16 kHz. We gradually increased the vibration frequency from 1.6 to 1000 Hz and obtained the sensitivity at discrete frequency points. For example, we fixed the frequency point at 10 Hz and recorded the $\mathbf{S_0}$ output (oscilloscope channel 1, Ch1) and the system's optical intensity (Ch2) with increasing the vibration amplitude. The Ch2 output was then converted into the phase delay of the LC cell and plotted with Ch1, as shown in Fig. 4(a). From the slope, we obtain the system's sensitivity of 0.0131 rad/mm/s. If we use the voltage output from the photodetector, V/mm/s as the unit, we need to consider the laser intensity and the detector sensitivity. Besides, we found that even at the lower limit of **VG**, vibration velocity of ~1mm/s, there was no significant distortion in the data points. Therefore, we infer that the resolution of the system is determined by PVT resolution and SNR. The upper limit of the system is determined by the TVC saturation of the HAN cell (~2V), as shown in Fig. 2(d), which is approximately 100 mm/s. Therefore, for application scenarios with strong vibrations, we can use PVT with lower sensitivity to ensure the system is within the range.

We checked the FR of S_1 in Fig. 4(b) (red dots), which is in accord with its catalog. There is a flat response from 10 to 500 Hz with a resonance at 80 Hz. The sensitivity at multiple frequencies constitutes the FR of the system, shown in Fig. 4(c). When detecting continuous vibrations, the relaxation time of the HAN cell affects the system FR, which was measured as 23.4 ms. Therefore, when the vibration frequency is greater than 42.7 Hz, LC molecules are driven again before returning to the initial position, resulting in sensitivity decay from ~40 Hz. In the low-frequency range, Fig. 4(b) clearly indicates that the sensitivity of the system (gray dots) is limited by the FR of PVT. Theoretically, LC can respond to DC signals, so the system's low-frequency response capability is blocked. Further confirmation of FR requires PVT and **VG** with better low-frequency performance. In summary, the HAN optical setup can achieve a response range of 0.1-50 Hz (± 10%), which covers the key frequency range of geological exploration and SHM.

In addition, we tested the system sensitivity dependence on the temperatures, as shown in Fig. 4(e). In the current stage, we only heat up the HAN cell to exclude variables generated by the laser and detector. The system sensitivity significantly depends on the LC refractive index, order parameter, K_{ii} at different temperatures. The system failed when the temperature reached the LC clearing point (T_{NI}). Therefore, the system has to be installed in a temperature-stable environment to maintain stable detection, such as underground or shield areas, which coincides with the installation principle of outdoor vibration detectors.

Similarly, we obtained the FR of HANG in Fig. 4(d). Its flat response range is similar to HAN. Differently, for grating, we focus on the light intensity of 0-order at different applied voltages, so we directly used the detector voltage output as the unit, ~16 mV/mm/s (@10 Hz). The sensitivity of the system is affected by the diffraction efficiency (DE) of grating, laser intensity, and detector sensitivity (0.3A/W @ 632nm, voltage divider resistance 20kΩ). If the pitch of the checkerboard is reduced, there is hope for further improvement in DE. Besides, the HANG modulator removes the polarizers, so it is an extremely low-cost solution.

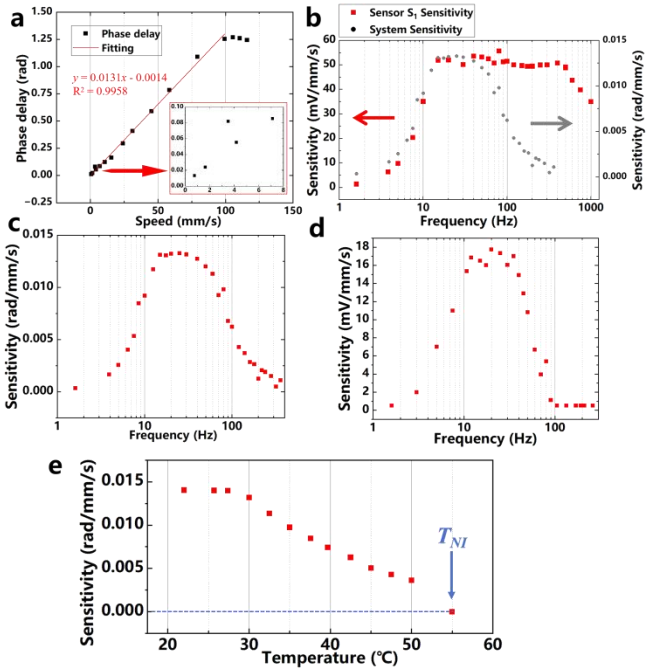

Figure 4. (a) Fixing at a frequency, the relation of HAN cell's phase delay and its vibration speed. (b) The FR of PVT S_1 and its overlap with the system FR. The FR of (c) the HAN cell system and (d) the HANG system. (e) The temperature dependency of a HAN cell system.

The system performance of natural vibrations sensing is a final capabilities test. As shown in Fig. 5(a), we chose a 130 × 70 × 2 cm^3 chipboard, with its four corners fixed. We installed a 941B ($\mathbf{S_2}$) connected to the HAN modulator at one corner of the board. We dropped a non-springy 50 g rubber block from different heights at the center to generate vibrations of varying magnitudes. The other referential 941B ($\mathbf{S'_0}$) was installed in a nearby location without contact to $\mathbf{S_2}$. The output from the system was recorded in Ch2, while the synchronous voltage output from $\mathbf{S'_0}$ was to Ch1. We converted Ch2 into phase and compared it with Ch1 in Fig. 5(b). By plotting the amplitude peaks of these 2 signals, we found that the system output had excellent linearity (Fig. 5(e)). In a vibration envelope with frequencies concentrated in 35-60 Hz, the system output exhibits slight distortion (dashed line in Fig. 5(c)). A HAN cell cannot follow the high-frequency part of the vibration signal, which performs like a DC component that generates a background phase delay from LC. So the phase output signal envelope is loaded with a small offset. Ignoring the offset, the response maintained a high linear reproduction of low-frequency signals (Fig. 5(d)). It proves the proposed system is suitable for vibration-amplitude-based modal recognition in SHM.

Similarly, we replaced the setup with a HANG set and recorded a vibration event, as shown in Fig. 5(f). The system can

reproduce the vibration envelope. However, due to the presence of 40-80 kHz noise from the laser, the output exhibits a low SNR. We calculated the power spectral density (PSD) of the signal and filtered >1kHz noise (Hamming window, overlap 50%, nfft = 262144). Fig. 5(g) clearly indicates that the system output (red) doubles the vibration's central frequency (black) and contains <50 Hz noise. Since NLC cannot distinguish positive or negative signals, a reciprocating vibration is responded twice by the system, doubling the original frequency. The low-frequency noise is caused by the fluctuation of laser intensity. After modifying the analysis model, the HANG system has the applicability of spectrum-based analysis in SHM. In the next stage, we will use more stable gas lasers to increase intensity stability and SNR. The HANG system removes the polarizers, significantly reducing the loss of light intensity and improving sensitivity. In addition, its highly cost-efficient and passive sensing characteristics ensure its feasibility as the nodes in large-scale sensor networks. For example, we can assemble multiple proposed systems into a sensing array and install it in buildings or on land. A high-density sensor network can locate the vibration source and digitally restore the vibration pattern. In the concept diagram of Fig. 5(h), sensor networks can achieve high-precision digital reconstruction of vibrations and display them in 3D on interfaces such as AR, VR, even restoring human body sensation, as a great tool in digital twins and metaverse.

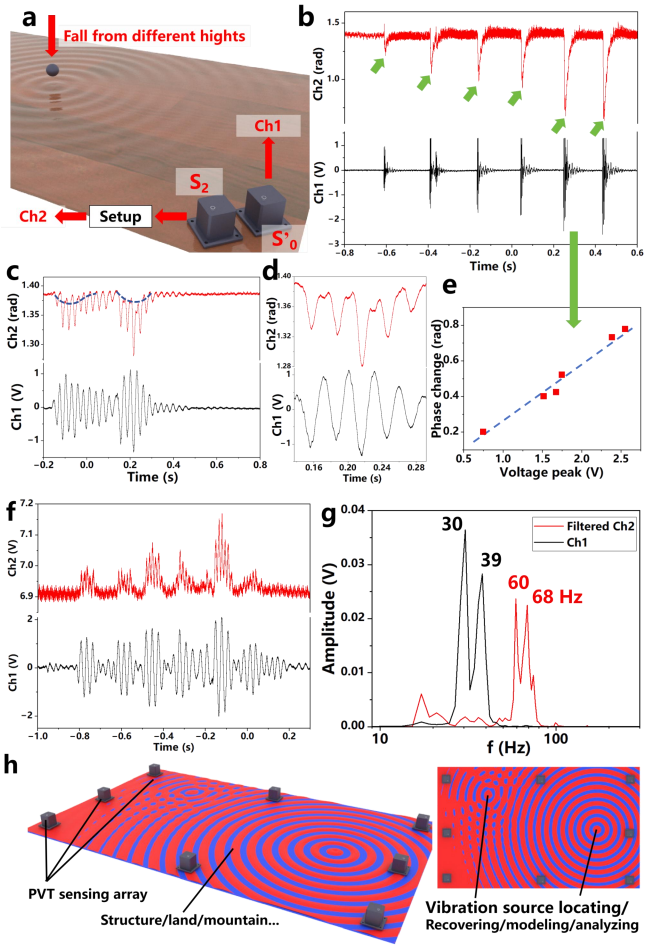

Figure 5. (a) The natural vibration generated by the ball is measured by the HAN system (Ch1) and reference PVT (Ch2). (b) Measured vibrations with increasing amplitudes. (c) The HAN system and reference output of a seismic event and (d) the enlarged different of them. (e) The linearity of peaks got from (b). (f) The HANG system and reference output of a seismic event and (g) their power spectrum density. (h) The concept of 3D vibration digital recovery realized by PVT sensing array.

The NLC-based system suffers from limited response speed and linear range. In the next step, we will seek a longer linear range and higher response speed. Additionally, to detect subtle accelerations of micro seismic events, such as building self-vibration and distant earthquake events, we will utilize PVTs with higher sensitivity, more powerful stable lasers, and more sensitive detectors to enhance sensitivity and SNR.

4. Conclusion

We successfully achieved passive vibration detection using threshold less HAN and HANG modulators. The proposed system achieved a sensitivity of up to 13.1 rad/m/s, 0.1-50 Hz FR, and smaller than one mm/s resolution comparable to the state-of-the-art vibration sensor. The system exhibits excellent vibration envelope reproducibility and linearity in the low-frequency range in vibration testing on simple structures. The lack of a power source at the sensor probe gives the proposed passive sensor a distinct edge over commercial vibration sensors. Through PSD analysis, we further confirmed its practicality in SHM analysis techniques based on vibration and spectrum.

5. Acknowledgments

We acknowledge the support of from The Government of the HK SAR, the Research Grants Council (RGC) for the grant 16205623, and Innovation and Technology Fund (ITF- ITS/059/22MX). We also acknowledge the support of The State Key Laboratory of Advanced Displays and Optoelectronics.

6. References

1. Ramírez-Moreno MA, et al. Sensors for sustainable smart cities: A review. App. Sci. 2021 Sep 3;11(17):8198.
2. Tiboni M, et al. A review on vibration-based condition monitoring of rotating machinery. Applied Sciences. 2022 Jan 18;12(3):972.
3. Bernas M, et al. A survey and comparison of low-cost sensing for road traffic monitoring. Sensors. 2018 Sep 26;18(10):3243.
4. Hassani S, et al. A systematic review of advanced sensor technologies for non-destructive... Sensors. 2023 15;23:2204.
5. Li M, et al. A high performance piezoelectric sensor for dynamic force monitoring of landslide. Sensors. 2017 Feb 17;17(2):394.
6. Zhao H, et al. A highly sensitive triboelectric vibration sensor for machinery condition... Adv. Ene. Mat. 2022 Oct;12(37):2201132.
7. Zhang Q, et al. Micro-fiber-based FBG sensor for simultaneous measurement of vibration and temperature. IEEE Photonics Technology Letters. 2013 Jul 11;25(18):1751-3.
8. Nishikawa T, et al. The slow earthquake spectrum in the Japan Trench illuminated by the S-net seafloor observatories. Science. 2019 Aug 23;365(6455):808-13.
9. Marra G, et al. Ultrastable laser interferometry for earthquake detection with terrestrial... Science. 2018 Aug 3;361(6401):486-90.
10. Goodby JW, et al, editors. Handbook of liquid crystals, 5 volume set. John Wiley & Sons; 2014 Apr 14.
11. Matsumoto S, et al. Field-induced deformation of hybrid-aligned nematic liquid crystals: New multicolor liquid crystal display. Journal of Applied Physics. 1976 Sep 1;47(9):3842-5.
12. Pozhidaev EP, et al. Orientational Kerr effect and phase modulation of light in deformed-helix ferroelectric liquid ... Phys. Rev. E—Stat. Nonlin. & Soft Mat. Phys.. 2013 May;87(5):052502.
13. Yu X, et al. P-92: Photo-sensitive Vertical Alignment Material with Room Temperature Dipcoating Technique. InSID Symp. Digest of Tech. Papers 2024 Jun (Vol. 55, No. 1, pp. 1743-1746.
14. Yu X, et al. Monomolecular vertical alignment layer with room temperature... J. of Mol. Liq. 2022 Dec 1;367:120535.